TU Delft

Delft University of Technology

Document Version
Final published version

Licence
Dutch Copyright Act (Article 25fa)

Citation (APA)
Guo, Y., Zhang, T., Ma, Y., Wang, T., Liu, Y., Ni, M., Ye, G., Wei, J., Fu, J., & Yu, Q. (2026). Interfacial self-debonding in a basalt-polyacrylamide hydrogel composite enabling significant shrinkage mitigation in cementitious systems. *Composites Part B: Engineering*, *325*, Article 113992. https://doi.org/10.1016/j.compositesb.2026.113992

Important note
To cite this publication, please use the final published version (if applicable).
Please check the document version above.

Copyright
In case the licence states “Dutch Copyright Act (Article 25fa)”, this publication was made available Green Open Access via the TU Delft Institutional Repository pursuant to Dutch Copyright Act (Article 25fa, the Taverne amendment). This provision does not affect copyright ownership.
Unless copyright is transferred by contract or statute, it remains with the copyright holder.

Sharing and reuse
Other than for strictly personal use, it is not permitted to download, forward or distribute the text or part of it, without the consent of the author(s) and/or copyright holder(s), unless the work is under an open content license such as Creative Commons.

Takedown policy
Please contact us and provide details if you believe this document breaches copyrights.
We will remove access to the work immediately and investigate your claim.

This work is downloaded from Delft University of Technology.

Composites Part B 325 (2026) 113992



Contents lists available at ScienceDirect

Composites Part B

journal homepage: www.elsevier.com/locate/compositesb



Interfacial self-debonding in a basalt-polyacrylamide hydrogel composite enabling significant shrinkage mitigation in cementitious systems

Yiqun Guo [a], Tongsheng Zhang [b,*], Yuwei Ma [a,**], Tao Wang [b], Yunpeng Liu [c], Mingxing Ni [d], Guang Ye [e], Jiangxiong Wei [b], Jiyang Fu [a], Qijun Yu [b]

[a] Research Center for Wind Engineering and Engineering Vibration, Guangzhou University, Guangzhou, China
[b] School of Materials Science and Engineering, South China University of Technology, Guangzhou, China
[c] State Key Laboratory of Silicate Materials for Architectures, Wuhan University of Technology, Wuhan, China
[d] Anhui Provincial Key Laboratory of Green and Low-Carbon Technology in Cement Manufacturing, Hefei, China
[e] Department of Materials and Environment (Microlab), Faculty of Civil Engineering and Geoscience, Delft University of Technology, Delft, the Netherlands

ARTICLE INFO

Keywords:
Hydrogel composite
Interfacial self-debonding
Polymer redistribution
Physical crosslinking
Internal curing
Autogenous shrinkage

ABSTRACT

Designing hydrogel-based composites for internal curing in cementitious systems remains challenging due to the persistence of polymer phases as discrete particles, which leads to hydrogel-related pore formation and reduces mechanical properties. In this study, a basalt-polyacrylamide hydrogel composite (BCPA) was engineered by introducing micron-sized basalt particles as physical crosslinking centers to construct a polymer-particle interface whose stability is responsive to the surrounding ionic environment. Upon exposure to the ion-rich cement pore solution, cation adsorption on basalt surfaces is proposed to weaken the original polymer-basalt association, leading to a proposed interfacial self-debonding process and inferred redistribution of polyacrylamide segments within the cement matrix. This interfacial evolution induces a transition of the polymer phase from a discrete particulate state to a dispersed segmental configuration, thereby altering the structural response of the hydrogel composite after incorporation. As a consequence, hydrogel-related marcopores are markedly suppressed. The inferred redistribution of polymer segments allows internal curing functionality to be retained while enabling a refined pore structure that can be readily accommodated by hydration products. At a dosage of 1 wt%, BCPA reduces 7-day autogenous shrinkage by approximately 75% and decreases cracking area by nearly one order of magnitude, while limiting compressive strength loss within 20%, substantially lower than the approximately 44% loss observed for the chemically crosslinked polyacrylamide reference (a typical internal curing agent). These findings suggest that regulating interfacial interactions to modulate polymer state evolution offers a promising strategy for designing hydrogel composites that reconcile shrinkage mitigation with mechanical integrity in cementitious systems.

1. Introduction

Adopting a low water-to-cement ratio is an effective approach to improve the strength and durability of cement-based materials, but it inevitably induces significant volume deformation, particularly autogenous shrinkage, which markedly increases the risk of early-age cracking [1–5]. Autogenous shrinkage primarily arises from the reduction of internal relative humidity caused by self-desiccation, as described by Laplace's equation and Kelvin's formula [6,7]. During cement hydration, the continuous consumption of free water leads to a progressive decrease in internal humidity, while the effectiveness of external curing is limited [8]. To mitigate shrinkage induced by self-desiccation, internal curing technologies have been extensively investigated to maintain internal moisture and sustain hydration [9,10]. Superabsorbent polymers (SAPs), as representative hydrogels with high water absorption capacity, are widely used as internal curing agents [11,12]. Water stored in typical hydrogels is gradually released into the cement paste due to the humidity gradient between the water-bearing polymer and the surrounding matrix. However, hydrogel-related pores generated after water release increase the porosity of the hardened

* Corresponding author.
** Corresponding author.
E-mail addresses: mstszhang@scut.edu.cn (T. Zhang), yuwei_ma@gzhu.edu.cn (Y. Ma).

https://doi.org/10.1016/j.compositesb.2026.113992
Received 13 April 2026; Received in revised form 29 June 2026; Accepted 13 July 2026
Available online 13 July 2026
1359-8368/© 2026 Elsevier Ltd. All rights are reserved, including those for text and data mining, AI training, and similar technologies.

matrix, exacerbate stress concentration, and facilitate crack propagation [13]. For instance, incorporating 0.6% hydrogel (acrylamide/acrylic sodium copolymer) into Portland cement paste was reported to compensate for approximately 68.4% of autogenous shrinkage, while simultaneously causing a 31.1% reduction in compressive strength [14], which has been attributed to the formation of hydrogel-related marcopores associated with water release. Recent studies further confirm that this strength penalty persists across different SAP chemistries, sizes, and dosages [15–17]. Despite differences in absorption kinetics or modified chemical compositions, the formation of hydrogel-related marcopores upon water release remains the dominant factor controlling the strength loss of hydrogel-modified cement matrix. It suggests that the origin of the strength penalty does not lie in any specific SAP formulation but in the persistence of the polymer phase as a discrete particulate state.

Recent advances in nanocomposite engineering have demonstrated that the incorporation of nanoscale additives can significantly enhance the mechanical performance, durability, and microstructural characteristics of cementitious materials. These improvements are primarily attributed to refined pore structure and improved interfacial interactions within the matrix [18,19]. Similar trends have also been observed in geopolymer-based systems, where nanomaterials contribute to enhanced structural integrity and long-term stability [20,21]. Despite these advances, hydrogel-based composites face additional design considerations because the polymer phase may simultaneously serve as a mechanical reinforcement and as a functional internal curing reservoir, making their structural response to the cement matrix more complex than that of conventional inorganic nanocomposites. The disparate mechanical properties between hydrogel and the cement matrix can lead to inconsonant deformation under stress, thereby promoting cracking [22]. To improve the mechanical compatibility of hydrogels, double-network hydrogel composites have been widely developed to enhance the intrinsic mechanical properties of the polymer phase [23,24]. In addition, reinforcing hydrogels with inorganic nanoparticles has been demonstrated as an effective strategy. Nano calcium hydroxide derived from the hydration of tricalcium silicate (C_3S) has also been employed during in situ polymerization of acrylamide, acting as linking nodes to improve the strength of hydrogel composites [25]. Similarly, montmorillonite was exfoliated into clay nanoplatelets and incorporated into polyacrylamide (PAM) hydrogel (10% by weight), then high fracture elongation and toughness respectively up to 11,800% and 10.1 MJ m^{-3} were obtained [26]. The introduction of nanoparticles during hydrogel preparation has demonstrated potential in reducing hydrogel-related porosity and thus lessening its negative impact on the mechanical properties of cement-based materials [12,27]. Further investigations revealed that incorporating nano-SiO_2 into hydrogel systems can promote the formation of additional hydration products to partially fill hydrogel-related marcopores, leading to improved late-age mechanical performance [28]. These findings suggest that increasing the content of reinforcing particles is beneficial for improving the intrinsic mechanical properties of hydrogel composites and the densification of cement-based materials. Moreover, the incorporation of nano-silica has been reported to enhance the swelling capacity of hydrogel composites due to its large specific surface area and strong interaction with water molecules [29,30]. Conversely, a high concentration of inorganic particles may reduce swelling capacity, since strong polymer-particle interaction effectively raise the overall crosslink density of the network and restrict chain mobility [31,32]. The crosslink density of hydrogel composite is affected by the content of chemical crosslinker, such as N,N′-methylene-bisacrylamide and epichlorohydrin [33,34]. Lower concentrations of chemical crosslinkers result in a lower crosslinking density, which enhances the pore-filling effect and mitigates strength reduction [29]. However, increasing the content of reinforcing particles while simultaneously reducing crosslinking density is inherently conflicting, as nanoparticles may also act as additional crosslinking centers during hydrogel formation. This intrinsic trade-off between mechanical reinforcement and water-retention functionality suggests that further enhancing the intrinsic strength of particulate hydrogels may not be the most effective route toward reconciling shrinkage mitigation with mechanical integrity in cementitious systems.

From the perspective of internal curing behavior, hydrogels are generally classified as non-retentive or retentive polymers [35]. Non-retentive polymers exhibit limited sensitivity to internal relative humidity and release absorbed water rapidly, resulting in relatively low efficiency in mitigating autogenous shrinkage [36]. In contrast, retentive polymers, such as polyacrylamide hydrogels, are capable of releasing water gradually and continuously, which is more effective in reducing shrinkage and associated strength loss [37,38]. Nevertheless, regardless of polymer type or reinforcement strategy, the polymer phase is generally treated as retaining its original dispersed or particulate form throughout the reaction process, then the formation of hydrogel-related macropores remains intrinsic to systems where the polymer persists as a discrete particulate phase. Building on the above convergent observations, we hypothesize that the existence state of the polymer phase, rather than its intrinsic mechanical properties, may govern how hydrogel-related marcopores develop and how the matrix accommodates internal curing in cement paste. If the polymer phase can be made responsive to the ion-rich pore solution environment such that it departs from its initial particulate state during mixing and hardening, the pore-related strength penalty intrinsic to particulate hydrogel may be mitigated without relying on further reinforcement of the polymer itself.

It should be noted that the cement pore solution is characterized by high alkalinity, high ionic strength, and enrichment of multivalent cations [39,40], which may directly interact with the polymer phase. However, the potential influence of this environment on the morphological state or physical existence of the polymeric component has received limited direct attention. Motivated by this conceptual gap, the present study explores an alternative approach to internal curing by examining the behavior of a physically crosslinked hydrogel composite in cement paste. A basalt-polyacrylamide hydrogel composite (BCPA) is employed, in which micron-sized basalt particles serve as physical crosslinking centers within a retentive polyacrylamide network. Rather than focusing solely on enhancing the intrinsic strength of hydrogels, this study investigates how such a composite interacts with the cement pore solution environment and how the state of the polymeric component may evolve after incorporation. The effects of the hydrogel composite on hydration behavior, microstructural development, mechanical properties, autogenous shrinkage, and cracking resistance of cement paste are systematically evaluated. It should be emphasized that the novelty of this work lies primarily in the conceptual reframing of how the polymer phase exists and evolves in the cement pore solution environment. This raises the central research question of whether the existence state of the polymer phase can be regulated through interfacial design to enable internal curing functionality while suppressing hydrogel-related pore formation in cement paste. Through this investigation, the study aims to provide insight into the relationship between polymer state, internal curing efficiency, and performance evolution, thereby offering a new perspective on the design of internal curing hydrogels for cement-based materials.

2. Experimental

2.1. Materials

It should be claimed that selecting basalt as the physical crosslinker in the present hydrogel composite was motivated primarily by its surface chemistry. The surface of basalt is enriched with silanol (Si–OH) and aluminol (Al–OH) groups [41], which provide multiple anchoring sites for hydrogen bonding and electrostatic interaction with the functional groups (e.g., $–CONH_2$ and $–NH_2$) of polyacrylamide chains, enabling the formation of a physically crosslinked polymer-particle interface. The chemical compositions of Portland cement (PC) and basalt (B), measured using X-ray fluorescence (XRF), are listed in Table 1. The

Table 1
Chemical compositions of Portland cement and basalt (wt%).

Material	SiO_2	Al_2O_3	Fe_2O_3	CaO	MgO	K_2O	Na_2O	SO_3	TiO_2	Others	LOI[a]
PC	20.21	5.00	4.21	61.21	1.09	0.72	0.24	2.77	/	1.24	2.23
B	45.34	15.71	11.77	8.45	5.45	/	4.35	2.61	2.34	1.62	2.36

[a] LOI, loss on ignition.

particle size distributions of cement and basalt were measured by laser diffraction method, as illustrated in Fig. 1. All chemical agents employed for hydrogel composite preparation, including acrylamide (AM), *N*, *N*′-methylene-bisacrylamide (BIS), potassium persulfate ($K_2S_2O_8$), sodium hexametaphosphate ($(NaPO_3)_6$) were analytically pure and used as received.

2.2. Sample preparation

The basalt-polyacrylamide hydrogel composite (BCPA) was prepared by crosslinking and gelation of acrylamide in the presence of suspended basalt particles, which acted as physical crosslinking centers, as detailed in Section 3. Portland cement paste without mineral or hydrogel additives served as the reference, and the dosage of BCPA was constant at 1.0. For comparison, cement pastes containing 1.0 wt% covalently crosslinked polyacrylamide (PAM) hydrogel or basalt particles were prepared to evaluate the individual contributions of polymer and mineral components. In addition, considering that the basalt content in BCPA was 13.6% (calculated as described in Section 3), a cement paste containing a physically mixed basalt-PAM system (0.14 wt% basalt particles and 0.86 wt% PAM) was prepared to clarify the effect of composite formation. As summarized in Table 2, the effective water-to-cement ratio (W/C_e), defined as the mass ratio of blending water to cement, was fixed at 0.30 for mixtures containing hydrogels. Additional water was introduced for pre-wetting the hydrogel to mitigate the loss of flowability caused by rapid polymer absorption, resulting in a pre-wetting water-to-cement ratio (W/C_p) of 0.05. Because basalt particles exhibited negligible water absorption, no pre-wetting water was applied, and their effective water-to-cement ratio was therefore treated as 0.35.

Hydrogel-containing additives were first mixed with deionized water according to the specified W/C_p and allowed to pre-wet for 1 h. The pre-wetted hydrogel was then incorporated during mixing of Portland cement and blending water. Fresh cement pastes were cast into molds with dimensions of 20 × 20 × 20 mm^3 and cured at 20 ± 1 °C and 95 ± 2% relative humidity. The specimens were sealed and cured at 20 ± 1 °C until the target age, followed by freeze-drying prior to microstructural characterization.

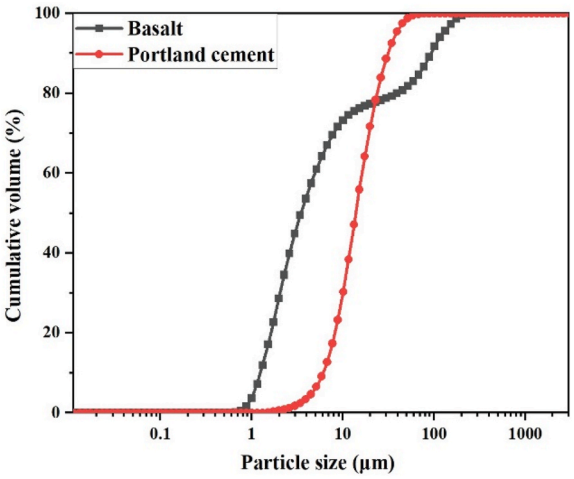


Fig. 1. Particle size distributions of Portland cement and basalt.

2.3. Testing methods

2.3.1. Swelling capacity measurement

The swelling capacity of PAM and BCPA hydrogel composite was determined using the tea-bag method [42]. Cement pore solution was used as the soaking medium to better simulate the actual chemical environment encountered in cement paste. The pore solution was obtained by centrifuging fresh cement paste and subsequently transferred into polypropylene bottles sealed with plastic film to prevent carbonation.

2.3.2. Compositions and microstructural characterizations

Thermogravimetric analysis (TGA) was performed using a Netzsch STA 449 thermal analyzer at a heating rate of 10 °C/min over a temperature range of 30-900 °C. Approximately 15 mg of sample was used for each measurement, with an empty corundum crucible as the reference and a nitrogen flow rate of 20 mL/min [43].

Fourier transform infrared spectroscopy (FTIR) was conducted on PAM, basalt, and BCPA hydrogel composite over a wavenumber range of 400-4000 cm^{-1} with a spectral resolution of 2 cm^{-1}. Prior to testing, 1 mg of sample was thoroughly mixed with 100 mg of KBr [44].

The morphology and elemental distribution of hydrogels and hardened cement pastes were examined using a scanning electron microscope (SEM) equipped with an energy-dispersive spectrometer (EDS). Samples were freeze-dried and gold-coated prior to SEM observation. Polished sections were prepared for backscattered electron (BSE) imaging and EDS mapping. Accelerating voltages of 10 kV and 20 kV were applied for morphology observation and BSE imaging, respectively.

X-ray powder diffraction (XRD) with Cu Kα (λ = 1.5406 Å) radiation was employed to determine the phase assemblage of cement paste, with scanning in the range of 5°-75° (2θ) at 0.013° per step.

Mercury intrusion porosimetry (MIP) was employed to characterize the pore structure of cement pastes. Freeze-dried samples were crushed into small fragments, and approximately 1.5 g of material (with a precision of 0.0001 g) was used for each test. The applied pressure ranged from 1.5 to 30,000 psi under incremental pressurization, with an equilibrium time of 10 s for each increment. The surface tension of mercury and contact angle were assumed to be 0.485 N/m at 25 °C and 130°, respectively [45]. Mercury intrusion porosimetry is subject to inherent methodological limitations, including the ink-bottle effect, possible high-pressure compaction of fine pores, and accessibility-dependent detection of isolated voids. Each MIP measurement was performed on one representative specimen per mixture, consistent with common practice in cement-based MIP study [9].

2.3.3. Determination of hydration behavior and properties of cement paste

The hydration heat evolution rate and the cumulative heat of cement pastes were measured using a TAM Air isothermal calorimeter at a constant temperature of 25 °C for 72 h.

Compressive strength was measured at curing ages of 3 and 28 days. Six cubic specimens (20 × 20 × 20 mm^3) were tested at a loading rate of 2.4 kN/s, and the average value was reported.

Autogenous shrinkage of cement pastes was continuously monitored over 7 days using a non-contact corrugated tube system [46]. Fresh cement paste was injected into corrugated tubes and carefully vibrated to eliminate entrapped air. The initial gauge length of the corrugated tube was approximately 250 mm with a precision of 0.1 mm. Three replicates were tested for each mixture, and the average value was

Table 2
Mix proportions of cement pastes containing hydrogel composite.

ID	Portland cement (%)	Dosage of additive			W/C_t	W/C_e	W/C_p	Superplasticizer (%)
		Basalt (%)	PAM (%)	BCPA (%)				
R	100	/	/	/	0.30	0.30	/	0.22
PA	100	/	1.00	/	0.35	0.30	0.05	0.22
B-PA	100	0.14	0.86	/	0.35	0.30	0.05	0.22
BCPA	100	/	/	1.00	0.35	0.30	0.05	0.22
BA	100	1.00	/	/	0.35	0.35	/	0.22

Note: W/C_t, W/C_e, and W/C_p are total water-to-cement ratio, effective water-to-cement ratio, and pre-wetting water-to-cement ratio, respectively.

reported. The initial setting time determined by the Vicat test was adopted as time zero for shrinkage measurements [47].

A restrained plastic shrinkage cracking test was conducted to evaluate the cracking resistance of cement paste. A self-designed mold with dimensions of 100 × 100 × 10 mm^3 was used, with bottom restraints provided by sixteen steel bars (Φ10 mm). After casting, specimens were cured at 20 ± 1 °C and 50 ± 5% relative humidity. Cracking resistance was evaluated based on the crack area ratio and the maximum crack width.

3. Results

3.1. Preparation and basic characteristics of basalt-polyacrylamide hydrogel composite

To enable basalt particles to act as physical crosslinking centers in the hydrogel composite, a stable suspension of basalt particles in an aqueous system was first established. Owing to the relatively large particle size compared with nanoparticles, basalt particles tend to sediment under gravitational force. Sodium hexametaphosphate ($(NaPO_3)_6$) was therefore employed as a dispersing agent to improve the dispersion stability of basalt particles by increasing their surface charge [48]. Specifically, a 1% $(NaPO_3)_6$ solution was prepared, and 4 g of basalt particles were dispersed in 20 mL of the solution under magnetic stirring for 20 min. After standing for 6 h, a stable basalt suspension was obtained by removing the slight sedimentation at the bottom. The median particle size of the suspended basalt particles was measured to be 3.8 μm by laser diffraction (Fig. 1). Acrylamide monomer was subsequently added to the suspension to achieve a monomer concentration of 4.0 mol/L. After magnetic stirring for 10 min, potassium persulfate ($K_2S_2O_8$) was introduced as the polymerization initiator at 0.6% molar ratio relative to the monomer. The mixture was stirred for an additional 20 min and then maintained at 60 °C for 2 h to complete polymerization and gelation. After removing edge portions, the resulting basalt-polyacrylamide hydrogel composite was obtained. The composite was freeze-dried to constant weight and ground to pass completely through an 80 μm sieve (Fig. 2). For comparison, a covalently crosslinked polyacrylamide (PAM) hydrogel was prepared using 4.0 mol/L acrylamide and 0.6% $K_2S_2O_8$, with 0.4% N,N′-methylene-bisacrylamide (BIS) introduced as a chemical crosslinker. The polymerization, gelation, freeze-drying, and grinding procedures for PAM hydrogel were identical to those applied to the basalt-polyacrylamide hydrogel composite.

SEM images of PAM and BCPA particles are presented in Fig. 3. Both hydrogels exhibited flake-like particle morphologies after grinding. EDS analysis showed that PAM particles consisted primarily of C, N, and O elements, whereas BCPA particles additionally contained Si and Al, confirming the incorporation of basalt particles into the hydrogel composite.

3.2. Composition of hydrogel composite

Owing to the slight sedimentation of basalt suspension, the actual content of basalt in BCPA hydrogel composite did not match the basalt concentration at the suspension stage. The actual basalt content in the BCPA hydrogel composite was determined by thermogravimetric analysis. PAM exhibited nearly complete mass loss at elevated temperatures, whereas basalt showed substantially higher thermal stability. Based on the distinct weight loss behaviors of PAM and basalt, the basalt proportion in BCPA was calculated using Eqs. (1) and (2). As illustrated in Fig. 4, basalt displayed slight and continuous weight loss below 600 °C, while the stepped weight loss of BCPA closely followed that of PAM. Three main weight-loss regions were observed at 60-140 °C, 250-300 °C, and 355-560 °C, respectively, consistent with dehydration and polymer decomposition processes [49,50]. According to the final mass losses, the basalt content in BCPA was calculated to be 13.6%.

$$w_{BCPA} = p_B \cdot w_B + (1 - p_B) \cdot w_{PAM} \quad (1)$$

$$p_B = \frac{w_{PAM} - w_{BCPA}}{w_{PAM} - w_B} \quad (2)$$

where, p_B was proportion of basalt in BCPA. w_{BCPA}, w_B, and w_{PAM} were the weight losses of BCPA, basalt, and PAM from 30 °C to 900 °C.

The FTIR analysis here is intended to establish the existence of interfacial interactions between basalt and polyacrylamide. FTIR spectra of basalt, PAM, basalt-PAM physical mixture (B-PA), and the BCPA hydrogel composite are shown in Fig. 5. The broad absorption band centered at 3471 cm^{-1} corresponds to O–H stretching vibrations, with additional contributions from N–H groups in PAM [51]. For basalt-containing samples, characteristic absorption peaks associated with Si–O-(Si or Al) bonds were observed at approximately 1010, 583, and 475 cm^{-1} [52]. PAM exhibited typical absorption bands corresponding to C–H stretching at 2924 cm^{-1}, C–N stretching near 1445 cm^{-1}, and C═O stretching around 1645 cm^{-1} [53,54]. Using basalt particles as physical crosslinking centers, the O–H adsorption band widened and shifted to a blue wavelength. Additionally, blue shifts

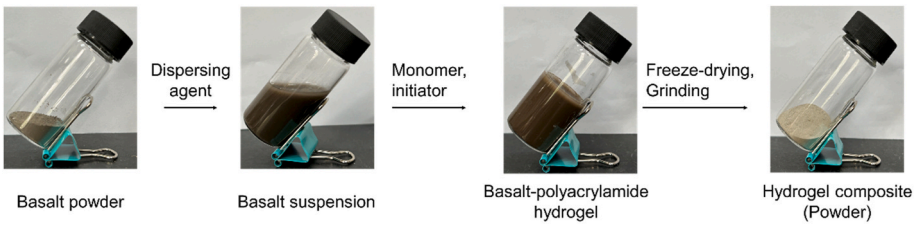


Fig. 2. Preparation process of basalt-polyacrylamide hydrogel composite.

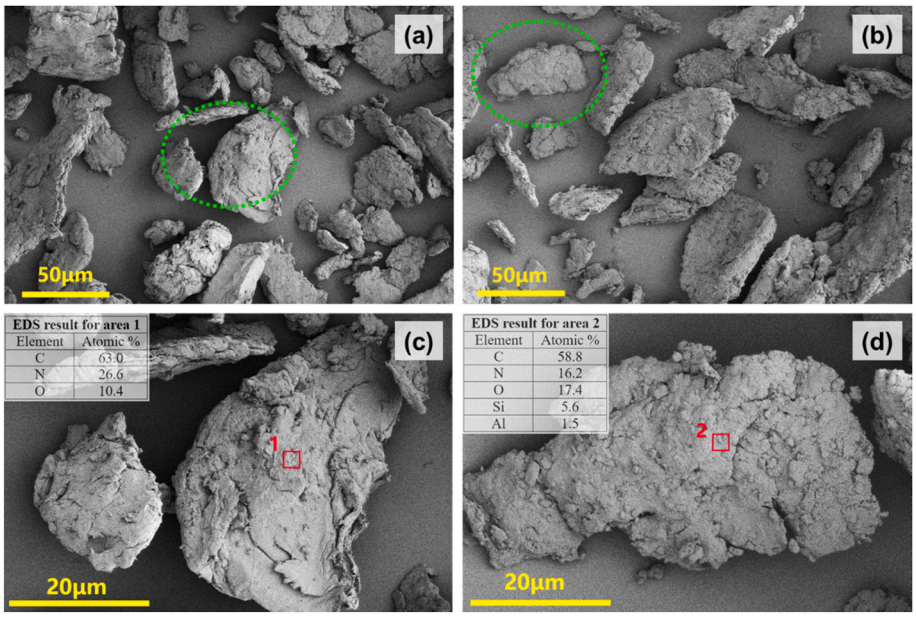


Fig. 3. The SEM images of PAM and BCPA particles: (a) PAM particles; (b) BCPA particles; (c) Enlarged view of PAM particles; (d) Enlarged view of BCPA particles.

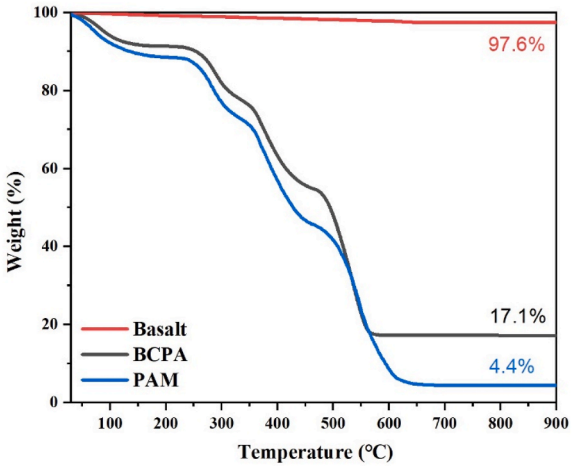


Fig. 4. The weight loss of basalt, PAM, and BCPA from 30 °C to 900 °C.

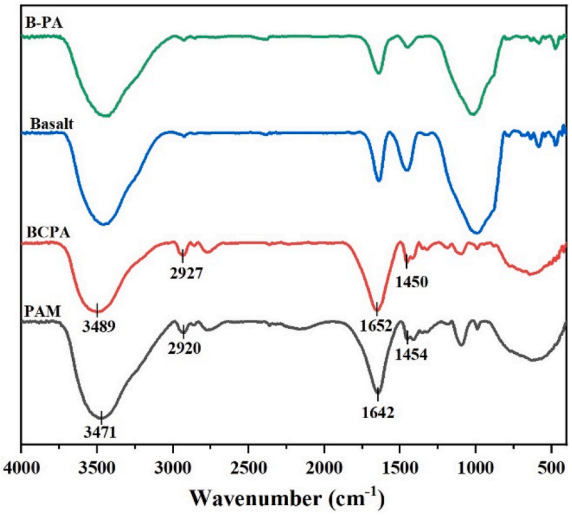


Fig. 5. FTIR spectra of basalt, PAM, B-PA mixture, and BCPA hydrogel composite.

in the C–H and C═O vibration peaks were observed, suggesting possible hydrogen-bond interactions between basalt and PAM. And the blue shifts observed in the O–H, C–H, and C═O bands were not present in the simply physically mixed basalt-PAM (B-PA) sample.

3.3. Swelling behavior of hydrogels in cement pore solution

The swelling behaviors of PAM hydrogel and BCPA hydrogel composite in cement pore solution are shown in Fig. 6. Both materials exhibited a rapid increase in swelling ratio at the initial stage, reaching approximately 50% of their equilibrium swelling capacity within the first 30 min. Subsequently, the swelling rate gradually decreased until equilibrium was attained. At equilibrium, the swelling ratio of PAM hydrogel was 20.1 g/g, whereas that of the BCPA hydrogel composite was 16.5 g/g, corresponding to a 17.9% reduction in swelling capacity for BCPA. The difference in swelling ratio between PAM and BCPA remained nearly constant throughout the swelling process, indicating a consistent disparity in water uptake behavior over time. Since basalt particles exhibit negligible water absorption and constitute 13.6% of the BCPA composite (section 3.1), the polymer phase available for water uptake in BCPA is correspondingly reduced. If the polymer network in BCPA retained exactly the same water-uptake capacity as the pure PAM hydrogel, the expected swelling ratio of BCPA would be approximately 17.4 g/g, based purely on the dilution effect. The measured value of 16.5 g/g is only about 4.3% lower than this dilution-corrected value (relative to the PAM baseline), indicating that the intrinsic water-uptake capacity of the polymer network in BCPA remains close to that of the pure PAM hydrogel. This suggests that the reduction in overall swelling is dominated by the dilution effect of the non-absorbing basalt phase rather than by a substantial alteration of the polymer network structure.

3.4. Hydration behavior of cement paste containing hydrogels

As illustrated in Fig. 7, the paste containing basalt exhibited a shortened induction period, ending at approximately 2.7 h, accompanied by a relatively high exothermic peak. In contrast, the incorporation of 1.0% PAM hydrogel led to a prolonged induction period, with the acceleration stage commencing at approximately 9.3 h and a noticeably

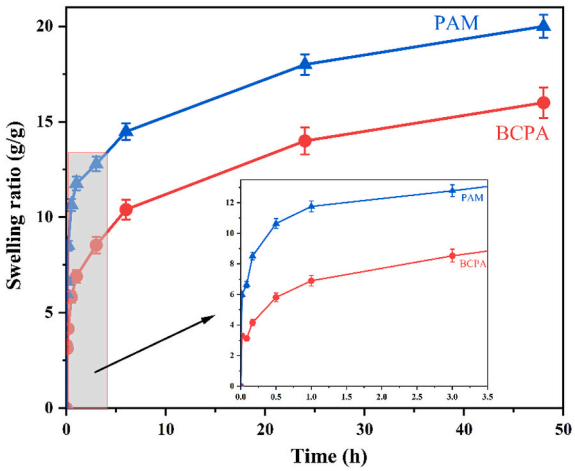


Fig. 6. Swelling ratios of PAM and BCPA in pore solution.

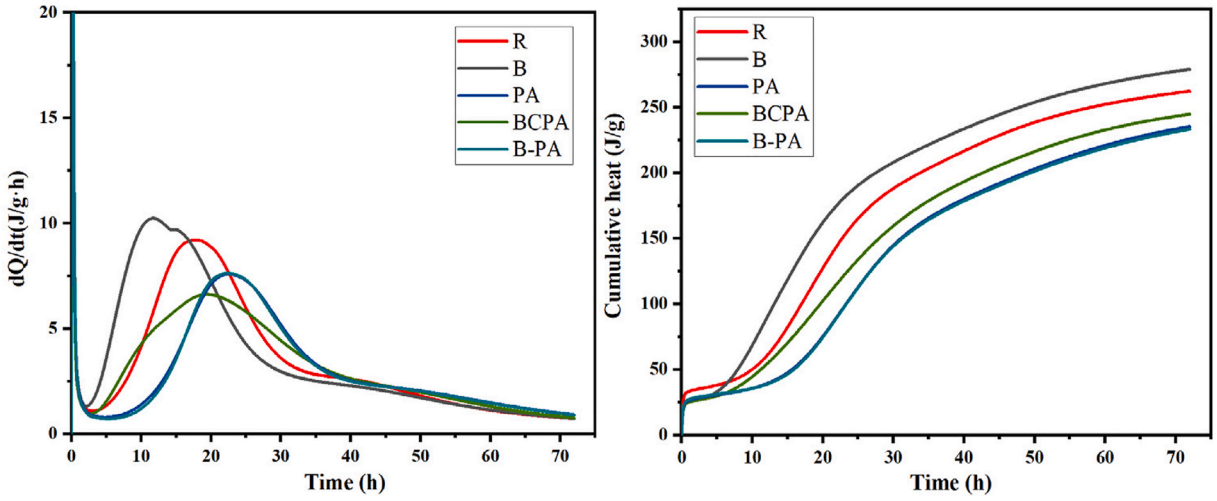
reduced exothermic peak compared with the reference cement paste. At 3 days, the cumulative heat of PAM was 236.3 J/g, which is 9.9% lower than that of Portland cement paste. The mix proportion of cement paste indicated a weight ratio of pre-wetted water to hydrogel ranging from 5.0 to 6.4, which significantly differs from the swelling capacity of hydrogel. Therefore, the pre-wetted hydrogel may continue to absorb a small amount of water, leading to a slight reduction in the effective W/C ratio and a delay in hydration. When basalt and PAM were combined, the hydration heat curve of B-PA nearly overlapped with that of PAM, suggesting that the heterogeneous nucleation effect of basalt can be neglected. With the BCPA hydrogel composite used in the cement paste, the onset of the acceleration period was close to that of Portland cement paste, in contrast to the pronounced delay observed for PA and B-PA. The exothermic peak of BCPA was lower than that of the reference paste, indicating that BCPA still exerted a certain retarding effect on cement hydration; however, this retardation was markedly weaker than that of PA and B-PA, being mainly reflected in a reduced peak intensity rather than in a delayed onset of acceleration. Additionally, the deceleration period lasted longer, and the delayed time to reach the stability period helped maintain the early-age hydration rate of the cement paste. Consequently, the cumulative heat of BCPA was only 6.7% lower than that of the control sample, compared with the 9.9% reduction observed for PA.

Thermogravimetric analysis was employed to characterize the hydration products of cement pastes at curing ages of 3 and 28 days, as shown in Fig. 8. At 3 days, pastes containing basalt or hydrogels exhibited higher total weight loss over the tested temperature range compared with the reference paste. Three main weight-loss regions were identified, corresponding to the removal of adsorbed water and decomposition of C–S–H, $Ca(OH)_2$ (CH), and calcite (Cc). Since calcite was not used in the raw materials, its formation is attributed to the carbonation of generated $Ca(OH)_2$. As illustrated in Fig. 4, the weight loss of the hydrogel mainly occurs in the range of 300-550 °C, which overlaps with the temperature window (380-470 °C) used for CH quantification and may lead to a slight overestimation of the CH content. Within the 380-470 °C window, the weight loss of BCPA was approximately 14.1% (Fig. 4). Given a BCPA mass fraction of about 0.85% in the hardened paste, the overestimated weight loss falling into the CH quantification window is approximately 0.12% of the paste weight, which is negligible and does not affect the comparison of CH contents among the pastes. At curing age of 28d, the higher C–S–H content in BCPA paste was more pronounced (Fig. 8b), indicating that there was no significant negative impact on hydration, even at later ages. In accordance with the weight loss related to decomposition of $Ca(OH)_2$ and calcite, the $Ca(OH)_2$ contents of cement pastes can be calculated theoretically [55]. Portland cement paste demonstrated slight lower $Ca(OH)_2$ content compared to pastes containing PAM, as reported by Yuan [56].

Beside the difference of hydration products content, the incorporation of BCPA hydrogel products also affected the crystal structure of products, especially the $Ca(OH)_2$. In Fig. 9, the (001) and (101) diffractions of $Ca(OH)_2$ (d-spacings of 4.9220 and 2.6270 Å) showed comparable intensities for the reference and basalt-containing pastes, whereas the relative intensities of these diffractions differed for the hydrogel-containing pastes, indicating a change in the preferred orientation of CH crystals. Consistently, the SEM images (Fig. 10) showed that CH appeared mainly as lamellar or plate-like crystals in the PAM-containing paste, whereas some rod-like CH crystals were observed in the BCPA-containing paste.

3.5. Mechanical properties and volumetric stability of cement paste

As illustrated in Fig. 11, the incorporation of basalt particles resulted in a reduction in compressive strength compared with the reference cement paste. At 3 days, the compressive strength decreased by



(a) Hydration heat evolution (b) Cumulative hydration heat

Fig. 7. Effects of basalt, PAM, B-PA mixture, and BCPA hydrogel composite on hydration process of cement pastes.

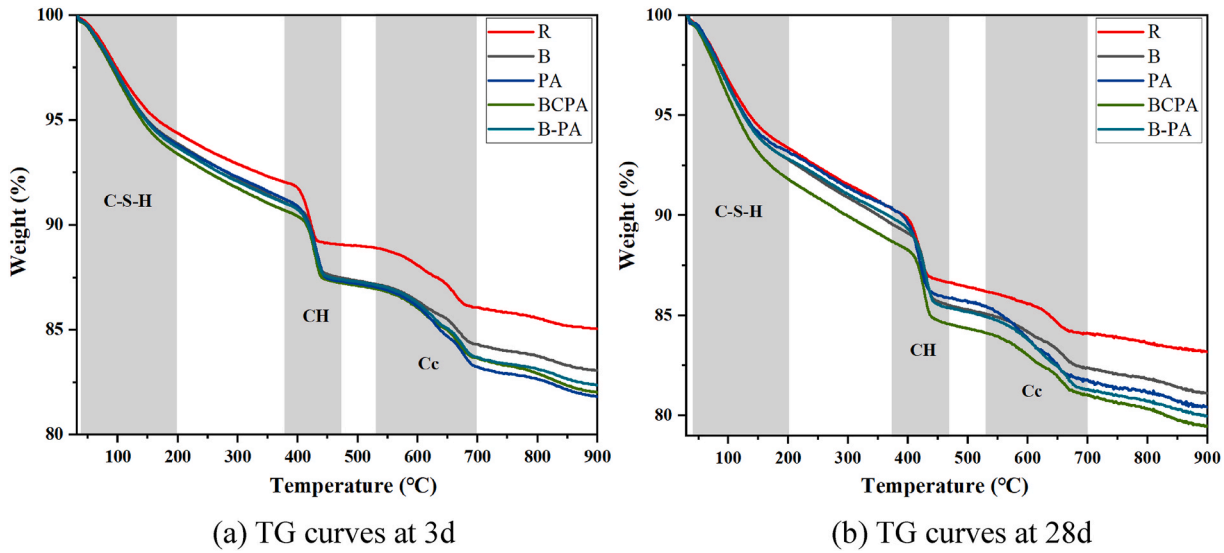


Fig. 8. Effects of BCPA hydrogel composite on weight loss of cement pastes.

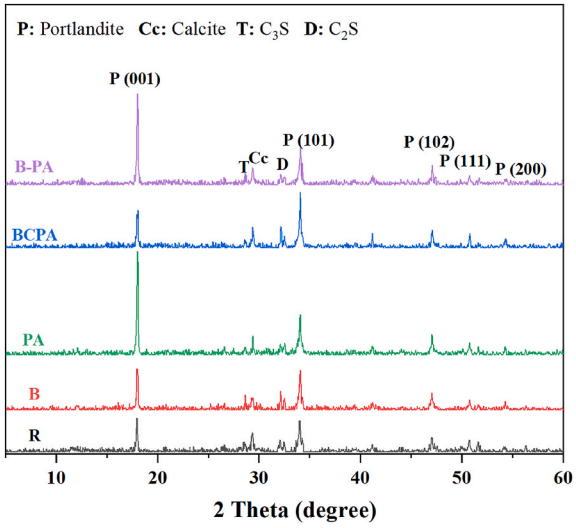


Fig. 9. XRD patterns of cement pastes at 3d

approximately 16.0%, which can be associated with the non-hydraulic nature of basalt and the increased effective W/C ratio. The introduction of 1.0% PAM hydrogel led to a pronounced reduction in compressive strength. The 3-day compressive strength of the PAM-modified paste was 38.8 MPa, corresponding to a reduction of 44.1% relative to the reference paste. Moreover, strength development after 3 days was limited, with the 28-day strength showing only a 20% increase compared to the 3-day compressive strength. Similar trends have been reported for cement pastes containing PAM-based internal curing agents [57]. When the basalt-PAM physical mixture was incorporated, the compressive strength at both 3 and 28 days was higher than that of the PAM-modified paste but remained lower than that of the reference paste. In contrast, the paste containing the BCPA hydrogel composite exhibited a substantially smaller reduction in compressive strength, and more pronounced strength development from 3 days to 28 days. The 28-day compressive strength of the BCPA-modified paste reached 73.1 MPa, corresponding to less than half of the strength reduction observed in the PAM-modified paste. The development of flexural strength followed a similar trend to that of compressive strength for all mixtures. The slighter strength loss in BCPA paste may be attributed to the refined pore structure compared with PAM paste, which would be further discussed in section 3.6.

The autogenous shrinkage of cement pastes measured over 7 days is presented in Fig. 12. Autogenous shrinkage of cement paste at very early ages is driven by chemical shrinkage, which is related to the hydration rate and affected by the mechanical properties of the paste. The rates of autogenous shrinkage of the tested pastes were nearly the same during the fast-growing stage (approximately within 10 h). However, the incorporation of pure PAM or PAM-containing mixtures led to a more pronounced increase in shrinkage. The hydration kinetics of cement paste showed that both PA and B-PA pastes had lower hydration rates, indicating delayed microstructure development and weaker mechanical properties, which resulted in larger deformations for PA and B-PA pastes during this period. Notably, a more significant expansion was observed in cement paste containing basalt compared to other specimens. Publication suggests that reabsorption of bleeding water and the oriented growth of crystal hydration products, such as ettringite and calcium hydroxide, may lead to volume expansion at an early age [58]. The higher effective W/C ratio of paste contained basalt inferred a greater bleeding risk. Additionally, the incorporation of basalt improved Ca

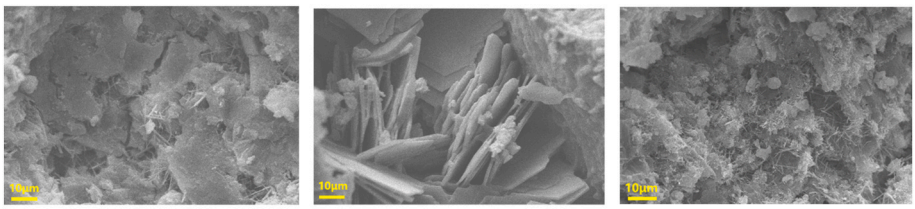


Fig. 10. SEM images of cement pastes at 3d

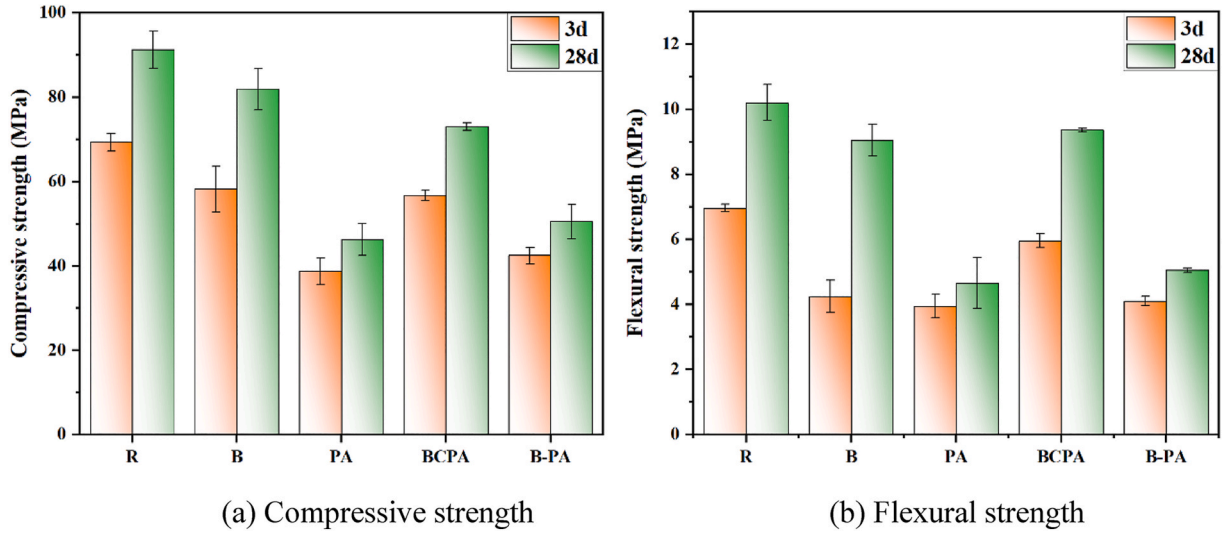


Fig. 11. Effects of BCPA hydrogel composite on mechanical properties of cement pastes.

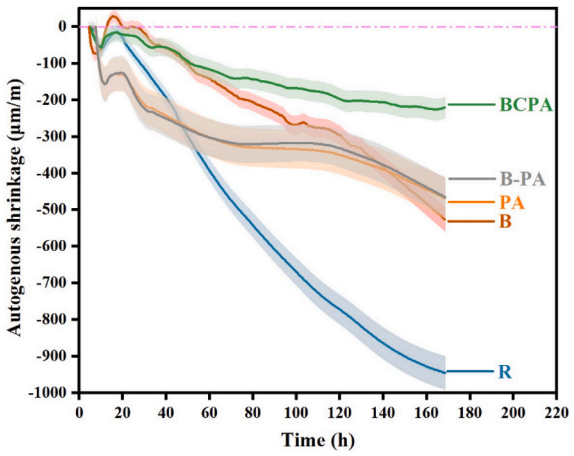


Fig. 12. Effects of BCPA hydrogel composite on autogenous shrinkage of cement pastes.

$(OH)_2$ generation compared with Portland cement paste, leading to higher internal stress due to crystal product growth. Although more Ca $(OH)_2$ was generated in PA and B-PA pastes, a slighter expansion was observed compared with BCPA paste. This may be attributed to the crystalline structure difference, where rod-like $Ca(OH)_2$ results in more pronounced stress from oriented crystal growth. After the expansion stage, cement pastes without hydrogel exhibited a rapid increase in shrinkage. With the introduction of hydrogel, the value and rate of deformations were limited, and the autogenous shrinkage of the hydrogel composite paste nearly leveled off after 120 h. At 168 h of curing, the autogenous shrinkage of Portland cement paste reached 946 μm/m, while the autogenous strains of pastes with PAM or PAM-containing mixtures were reduced to 468 μm/m. The effectiveness of PAM in mitigating shrinkage has also been reported in the literature [59]. Incorporating the BCPA hydrogel composite demonstrated a 75.9% reduction in shrinkage compared to Portland cement, the deformation development of the BCPA-modified paste tended to level off after approximately 120 h, indicating a distinct evolution of volumetric stability compared with the other mixtures.

To contextualize the present results against reported SAP-modified cementitious systems, the 75.9% reduction in 7-day autogenous shrinkage achieved by BCPA is higher than several recently reported values under similar low water-to-cement conditions. Approximately 28.6% shrinkage reduction after 7-day hydration was reported using acrylic acid-co-acrylamide hydrogel [60], and autogenous shrinkage reduction of 61.4% was published using hydrogel combined with modified cement particles [9]. Notably, incorporation of BCPA limits the compressive strength loss to about 20%, substantially less than the approximately 44% loss observed for the chemically crosslinked polyacrylamide reference, indicating that regulating polymer-particle interfacial interactions provides a competitive route to reconciling shrinkage mitigation with mechanical integrity, distinct from approaches relying on chemical modification of hydrogel particles or hybridization with highly reactive fillers.

The cracking behavior was evaluated through the restrained plastic shrinkage cracking test, and the cracking characteristics were assessed semi-quantitatively using the cracking area proportion and the maximum crack width as indicators, enabling a direct comparison among the different mixtures. In Fig. 13, the reference cement paste exhibited multiple interconnected cracks around the restraint elements, resulting in a cracking area proportion of 3.85% and a maximum crack width of 524 μm. This suggests higher internal stress and greater brittleness without hydrogels. When 1% PAM hydrogel was introduced, cracks were primarily located around partial restraint columns and were not continuous, indicating reduced sensitivity to restraint effects. The cracking area proportion decreased to 1.44%, attributed to the flexible nature of the introduced polymer [61]. When added basalt-PAM mixture, the amounts and distribution of cracks did not show significant differences compared to paste with pure PAM hydrogel. The paste incorporating the BCPA hydrogel composite exhibited the lowest cracking sensitivity among all mixtures. Only a limited amounts of short and narrow cracks were observed, with a maximum crack width of 235 μm. The cracking area proportion of the BCPA-modified paste was reduced by approximately one order of magnitude compared with that of the reference paste. The paste containing the basalt-PAM physical mixture did not show a comparable reduction in cracking sensitivity.

3.6. *Pore structure and polymer distribution in hardened cement paste*

The pore structure characteristics of cement pastes were investigated by MIP test, as shown in Fig. 14. At both 3 and 28 days, the reference cement paste exhibited the lowest total porosity among all mixtures as expected. The incorporation of basalt particles resulted in an increased porosity, particularly at 28 days. The introduction of PAM hydrogel or basalt-PAM mixture led to a pronounced increase in total porosity at 3 days. The porosity of the paste containing 1.0% PAM hydrogel reached 25.4%, compared with 20.1% for the reference paste. With increasing

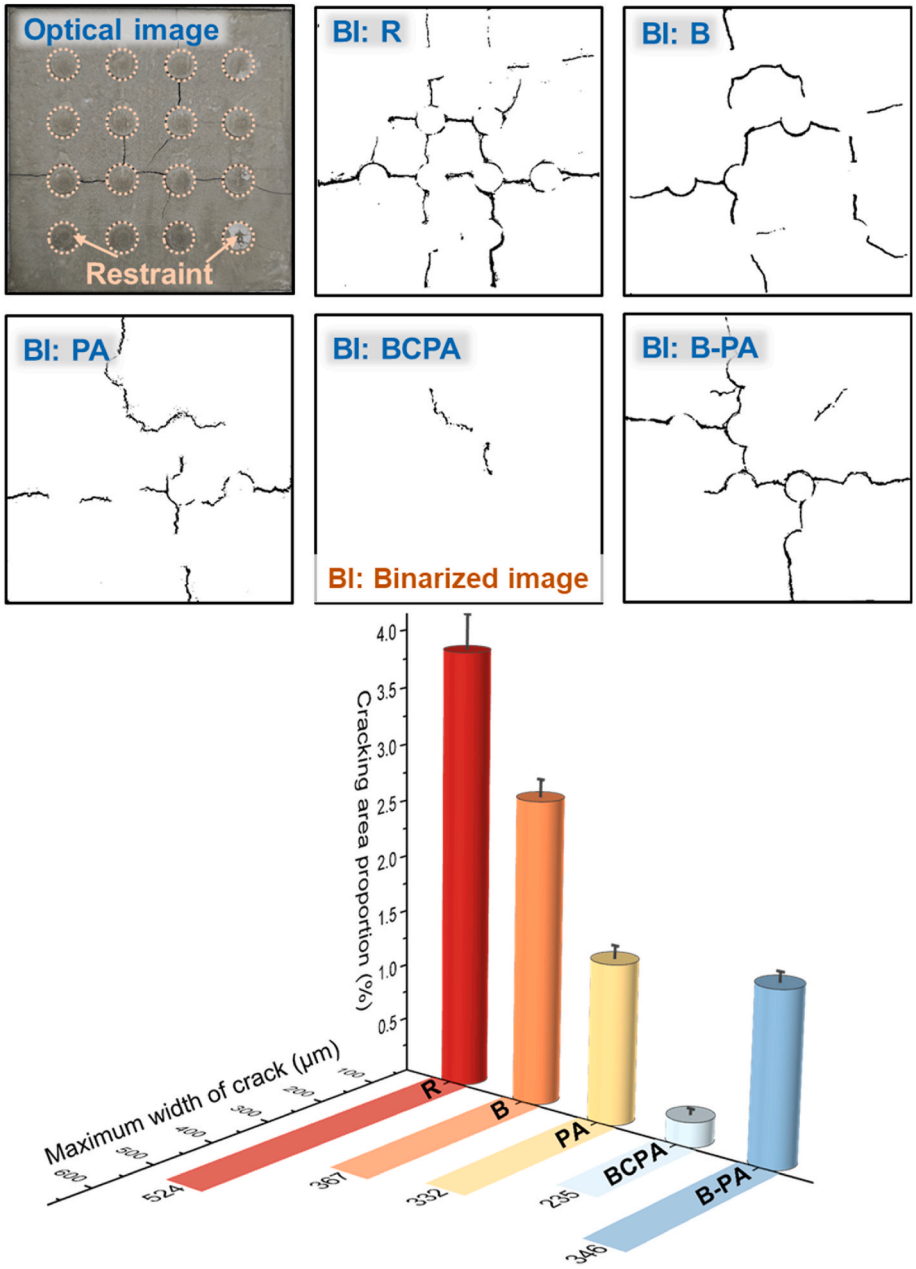


Fig. 13. Effects of BCPA hydrogel composite on cracking sensitivity of cement paste (Up: Cracking area proportion and maximum width of crack; Down: Optical and binarized images of cement pastes after restrained plastic shrinkage cracking test).

curing age, the porosity difference between the hydrogel-containing pastes and the reference paste decreased, indicating a gradual evolution of the pore structure over time. In contrast, the porosity of the paste containing the BCPA hydrogel composite did not exhibit a significant increase relative to the reference paste at either curing age. As for the pore size distribution of cement pastes illustrated in Fig. 14b, at both 3 and 28 days, the most probable pore size of the paste containing basalt was larger than that of the reference paste. For pastes incorporating PAM hydrogel or the BCPA hydrogel composite, a refinement of the pore structure was observed at early age, with the most probable pore size at approximately 13 nm at 3 days, compared with approximately 31 nm for the reference paste. At 28 days, the most probable pore size of the paste containing the BCPA hydrogel composite further decreased to approximately 11.1 nm. Notably, a broad pore size distribution extending beyond 50 μm was observed in the pastes containing PAM hydrogel or the basalt-PAM mixture, whereas such a pronounced macropore proportion was not detected in the paste containing the BCPA hydrogel composite. It is widely accepted that saturated polymer particles collapse in volume after water release, creating micron voids between the cement matrix and polymer particles, and the pores distributed at such size range usually have negative impact on the mechanical properties of cement paste [62]. In other word, the macropores caused by significant collapse of PAM-based materials cannot be eliminated completely, although hydrated might be promoted due to released moisture. On the contrary, when the BCPA hydrogel composite was introduced, the macropore proportion associated with hydrogel collapse was markedly suppressed, showing a notable difference compared with the pastes containing basalt or PAM individually.

As illustrated in Fig. 15, the microstructure of Portland cement paste was homogeneous, with only a few pores, represented by black regions in the BSE image. After incorporating basalt, the amounts of pores increased as expected, due to the lower strength and negligible

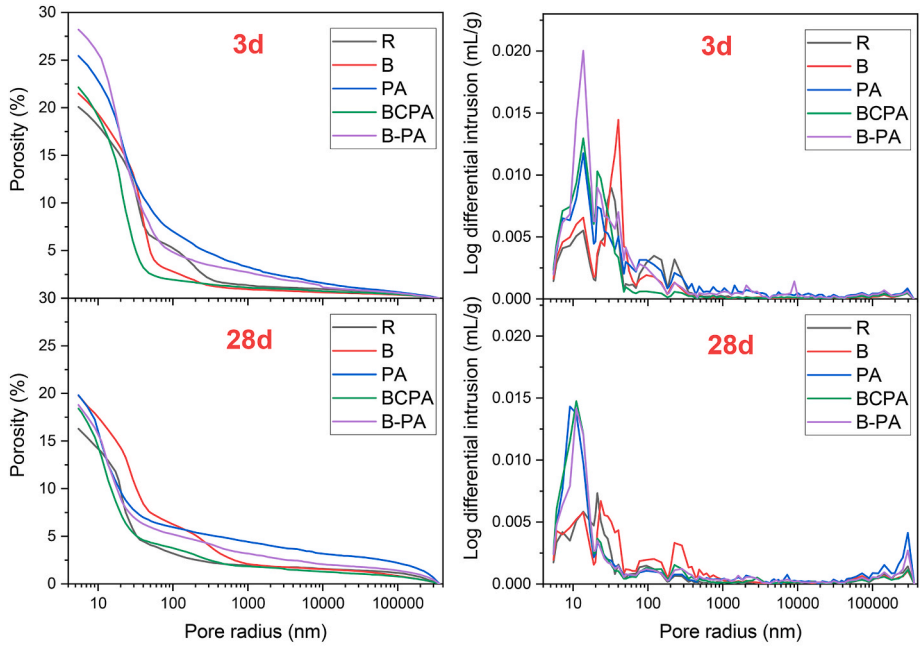


Fig. 14. Effects of BCPA hydrogel composite on pore structure of cement paste.

hydraulic activity of basalt. For the paste containing PAM hydrogel, two distinct features were identified: a relatively dense cement matrix and the presence of discrete hydrogel-related macropores. On one hand, hydration was promoted by water released from PAM hydrogel, leading to further densification of the cement paste. On the other hand, the significant volume collapse of PAM particles resulted in interfacial debonding. Although new hydration products formed at the original interface due to the promoted hydration, the space could not be completely filled. This is consistent with the increased micropore proportion in the cement paste (Fig. 14a). In contrast, the paste containing the BCPA hydrogel composite exhibited a more homogeneous, in which pronounced hydrogel-related marcopores were not observed. Carbon

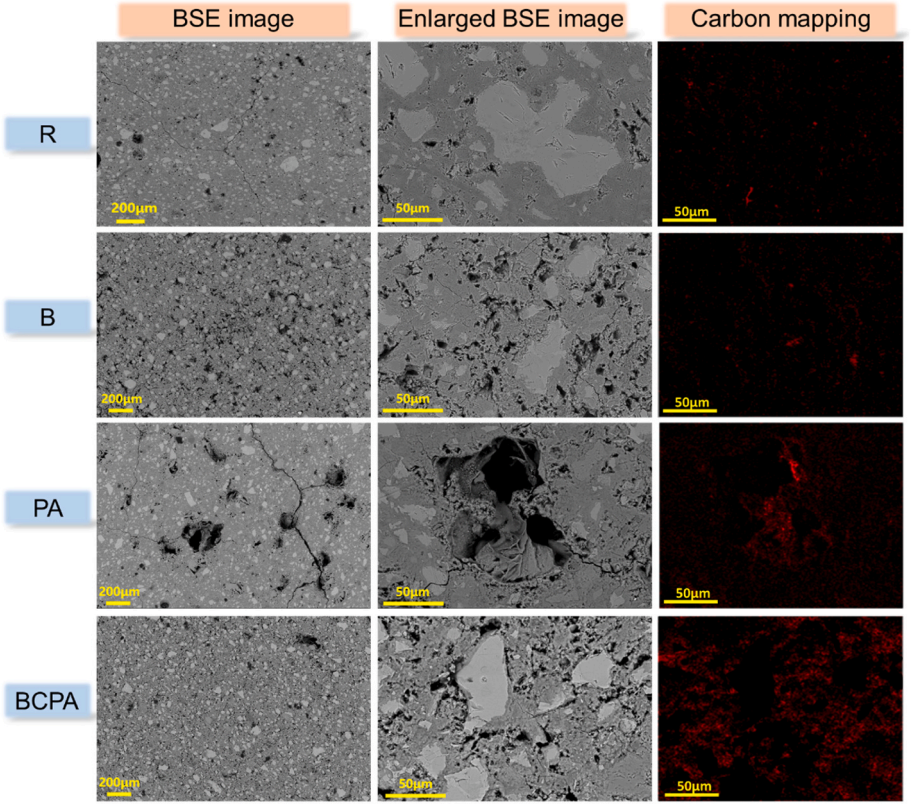


Fig. 15. BSE images and carbon mapping of cement pastes.

mapping showed that carbon was distributed more uniformly throughout the hydrated matrix, without the large, continuous carbon-rich domains seen in the PAM system. This indicates that the polymer phase in BCPA is no longer present as discrete particle-scale domains, but is distributed at a markedly smaller scale than the original composite particles.

4. Discussion

4.1. Self-debonding of basalt-polyacrylamide hydrogel composite

The experimental results indicate that the behavior of the basalt-polyacrylamide hydrogel composite in cement paste deviates from that expected for conventional particulate superabsorbent polymers. Compared with chemically crosslinked PAM, BCPA exhibits a reduced swelling capacity in pore solution while maintaining comparable swelling kinetics, and its incorporation does not lead to a pronounced retardation of cement hydration. These observations suggest that the polymer phase in BCPA does not function as a mechanically intact and persistent hydrogel particle after incorporation.

In BCPA, basalt particles act as physical crosslinking centers through non-covalent interactions with polyacrylamide chains, in contrast to the permanent covalent junctions present in chemically crosslinked PAM hydrogels. Such physically associated interfaces are inherently sensitive to the surrounding chemical environment. In cementitious systems characterized by high alkalinity and elevated ionic strength, especially in the presence of multivalent cations, modifications of interfacial interactions are therefore expected to occur. This environmental sensitivity was directly examined by tracking the morphological evolution of the hydrogels using optical microscopy. The PAM hydrogel and the BCPA composite were separately dispersed in deionized water and in cement pore solution by stirring the mixture for 5 s. A droplet of each suspension was immediately transferred onto a glass slide and observed as the initial state, and the suspension was then stirred for 2 min before a second droplet was sampled and observed. As shown in Fig. 16, the BCPA composite exhibited a clearly defined particle boundary of several tens of micrometers in deionized water, which was retained after stirring, whereas in the pore solution its initially discernible particle outline disappeared after stirring, with no obvious particulate form remaining. In contrast, the chemically crosslinked PAM hydrogel retained a clear particle boundary in both deionized water and pore solution, showing no comparable change. This contrast indicates that the loss of the particulate form is specific to the physically crosslinked BCPA composite and occurs only in the ion-rich pore solution, providing direct visual evidence that the physical polymer-basalt interface is destabilized in the pore solution environment.

The electrical conductivity results provide indirect evidence supporting this interpretation. As shown in Fig. 17, the introduction of chemically crosslinked PAM into pore solution leads to a slight decrease in conductivity, which is consistent with the ability of intact hydrogel particles to immobilize ions within their polymer network. In contrast, incorporating the BCPA hydrogel composite results in a pronounced increase in solution conductivity. This behavior suggests that the polymer phase in BCPA does not act as a closed, ion-blocking hydrogel particle, but instead allows ions to migrate more freely through the system. Such a difference in ionic transport behavior implies a marked change in polymer state compared with conventional particulate hydrogels.

Additional insight into the origin of this behavior is provided by the zeta potential measurements of basalt particles in different aqueous environments. As shown in Fig. 18, the surface potential of basalt shifts markedly in alkaline and ion-rich solutions, with a more pronounced positive shift observed in pore solution compared with NaOH solution of similar pH. The potential of basalt in deionized water was −20.57 mV. The silanol (Si–OH) or aluminol (Al–OH) groups on the basalt surface partially dissociate to form negatively charged groups ($Si–O^-$ or $Al–O^-$). In NaOH solution, abundant Na^+ ions cause these negative groups to adsorb cations, resulting in a significant positive shift in zeta potential. Unlike NaOH solution, the cations in pore solution are mainly divalent Ca^{2+}, with minor Na^+, K^+, and Al^{3+}. Polyvalent cations with higher charge density are more easily adsorbed than univalent cations, effectively neutralizing negative surface charges and reducing the system's total energy, leading to a more pronounced positive shift in potential. The adsorbed cations pair with the hydroxyl groups on the basalt surface to form Si–O–Ca^+ or Si–O–K, occupying the binding sites for polyacrylamide chains thereby weakening the non-covalent polymer-basalt association. Available studies have demonstrated that Ca^{2+} ions can strongly complex with amide-containing polymers and significantly influence polymer conformation and interfacial behavior [63,64]. In the present system, the combined effects of cation adsorption on basalt surfaces and Ca^{2+}-polymer interactions are therefore expected to

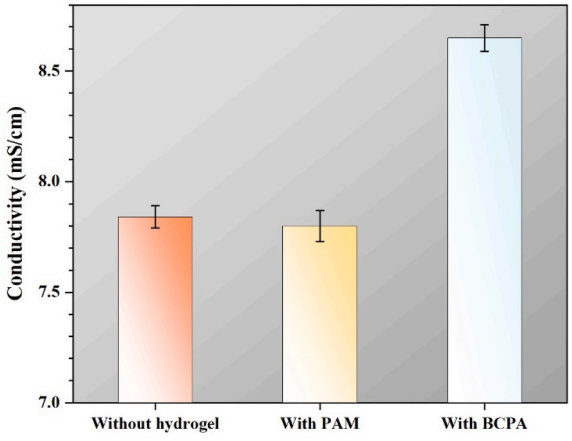


Fig. 17. Electrical conductivity of pore solution with and without hydrogel.

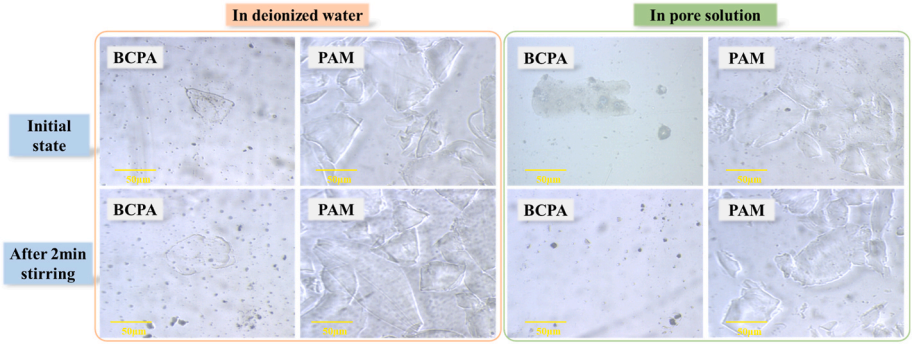


Fig. 16. The morphology evaluation of BCPA and PAM hydrogels in deionized water and pore solution.

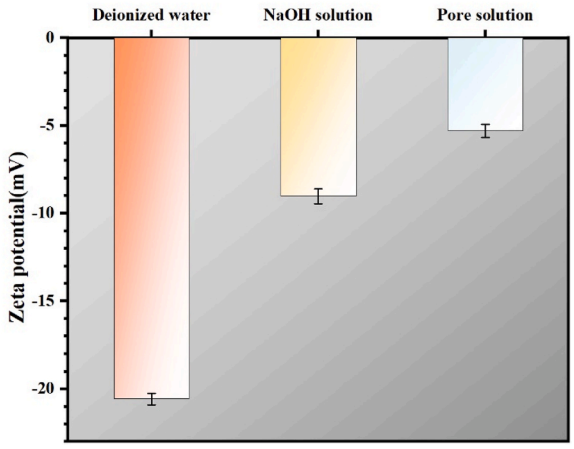


Fig. 18. Zeta potential of basalt in different aqueous solutions.

destabilize the original polymer-basalt interface. This process may lead to a gradual interfacial self-debonding, in which polymer chains detach from their initial particle-scale anchoring points without the need for external mechanical disruption. The distinct self-debonding behavior of BCPA cannot be attributed to mechanical fragmentation during mixing, since the basalt-PAM physical mixture subjected to the same process behaved like the PAM system rather than suppressing macropores, nor to polymer dissolution, since the internal curing performance was retained.

As a consequence of such interfacial evolution, the polymer phase is no longer confined to the spatial scale of the original composite particles and tends toward a more dispersed distribution within the cement paste during mixing and early hydration. It is emphasized that this redistribution does not imply complete dissociation of the polymer phase. Rather, it reflects a transition away from a particulate hydrogel state toward a non-particulate polymer presence, governed by environmentally induced changes at the polymer-particle interface.

4.2. Mitigation of hydrogel-related marcopores

The structural implications of the interfacial evolution discussed above can be directly examined through the pore structure and microstructural characterization results. In conventional SAP-modified cement systems, swollen hydrogel particles release stored water during hydration and subsequently undergo volumetric contraction. This particle-scale collapse typically generates hydrogel-related macropores, commonly in the tens of micrometers range, which originate from the spatial boundaries of intact hydrogel domains and are widely recognized as a major source of strength reduction.

The MIP results reveal a distinct contrast between pastes containing chemically crosslinked PAM and those incorporating the BCPA hydrogel composite. The PAM-modified paste exhibits a noticeable pore population in the macropore region, consistent with the collapse of discrete hydrogel particles. In contrast, although the overall porosity of the BCPA-modified paste is not completely unchanged, the characteristic macropore band associated with hydrogel-related macropores is markedly suppressed. The most probable pore size of the BCPA paste remains in the fine pore range and does not display the pronounced large-pore contribution observed in the PAM system. This indicates that the particle-scale cavities typically formed by hydrogel collapse are significantly mitigated when BCPA is introduced. Moreover, the paste containing PAM hydrogel presents spatially localized carbon-rich regions that coincide with distinct interfacial voids, reflecting the presence of discrete polymer domains and their associated debonding zones. By contrast, in the BCPA-modified paste, carbon is distributed more homogeneously throughout the hydrated matrix, and no distinct macropores corresponding to original composite particle boundaries are observed. The absence of concentrated carbon domains suggests that the polymer phase is not retained as intact hydrogel particles after incorporation, but instead exists in a more dispersed form.

It may be inferred that, if polymer chains detach from basalt particles and redistribute at a scale smaller than the original composite granules, the spatial extent of polymer contraction after water release would be correspondingly reduced. Rather than generating large particle-sized voids, polymer shrinkage would give rise to finer voids that are more readily accommodated or filled by ongoing hydration products. This redistribution-driven reduction in characteristic pore scale provides a rational explanation for the mitigation of hydrogel-related macropores observed in the BCPA system. Therefore, a conceptual evolution of BCPA in cement paste is proposed and schematically illustrated in Fig. 19. The schematic describes a three-stage scenario that is consistent with the combined physicochemical and microstructural observations, rather than representing a directly observed sequence. In Stage I, the BCPA composite exists as physically crosslinked granules, with basalt particles serving as crosslinking centers for polyacrylamide chains through hydrogen bonding and interfacial interactions. At this stage, the composite behaves as a particulate hydrogel entity, whose swollen size after pre-wetting can exceed the original dry particle size inferred from swelling capacity measurements. Stage II corresponds to the exposure of the composite to the actual cement paste, which with highly alkaline and ion-rich cement pore solution. Multivalent cations, particularly Ca^{2+}, preferentially adsorb onto surface hydroxyl groups of basalt (e.g., Si–OH and Al–OH), leading to a pronounced shift in surface potential and competitive occupation of interfacial bonding sites. This ionic shielding effect weakens the original hydrogen-bonding interactions between basalt and polyacrylamide chains. As a result, interfacial self-debonding may occur, and polymer chains detach from their bonding sites. The detached polymer segments are no longer constrained by the original composite boundaries and can redistribute within the cement paste during mixing and early hydration. In Stage III, after detachment from basalt surfaces, the dispersed polyacrylamide segments remain capable of absorbing and subsequently releasing water, thereby preserving the internal curing function typical of SAP systems. However, because the polymer no longer collapses as a large, discrete particle, the volumetric contraction after water release occurs at a smaller spatial scale. The voids generated by polymer shrinkage are therefore finer and more readily compensated by the formation and growth of hydration products, enabling the dispersed polymer to function as an internal curing agent without generating particle-scale pores.

The BCPA hydrogel composite exhibits a pronounced mitigation of autogenous shrinkage and reduced cracking sensitivity while avoiding the severe strength loss commonly associated with conventional particulate SAP systems. Unlike chemically crosslinked polyacrylamide hydrogels, which generate hydrogel-related macropores due to particle-scale swelling and collapse, the BCPA system undergoes interfacial self-debonding followed by polymer redistribution after incorporation into cement paste. This transition shifts the polymer phase away from a discrete particulate state and reduces the spatial scale of contraction during water release. The redistributed polymer segments retain their internal curing ability, the absence of large hydrogel domains significantly mitigates macropore formation. The resulting finer void structure can be more readily accommodated by hydration products, thereby limiting microstructural deterioration. In this regard, although BCPA exhibits a slightly lower equilibrium swelling ratio than PAM, its internal curing effectiveness is not diminished, because the internal curing efficiency depends not only on the water absorption capacity but also on how the polymer is distributed within the matrix. The more finely distributed polymer in BCPA releases water over a smaller spatial scale that better matches local self-desiccation, while avoiding the particle-scale macropores associated with the collapse of discrete PAM particles. Within this framework, the improved volumetric stability and preserved mechanical performance arise from polymer state transformation rather than simple additive reinforcement.

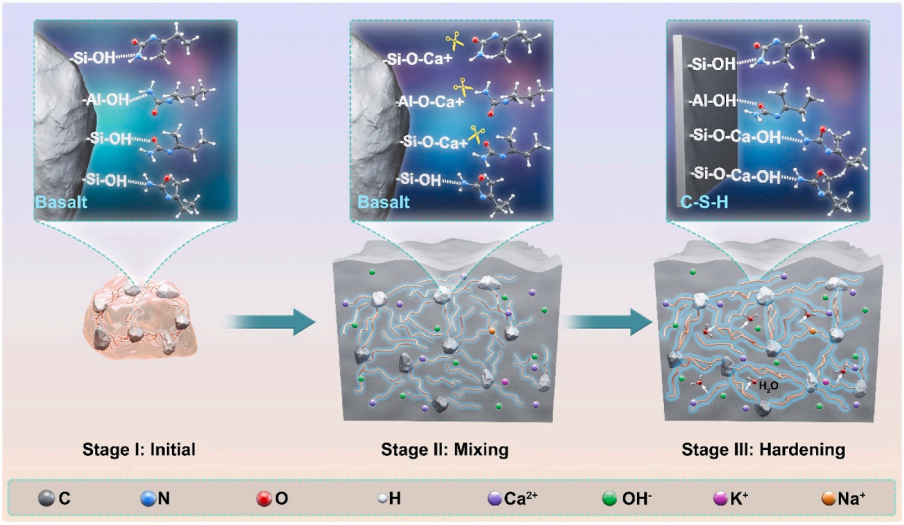


Fig. 19. Schematic illustration of the conceptual morphological evolution of the BCPA hydrogel composite in cement paste.

5. Conclusions and prospects

This study addressed the strength reduction commonly associated with conventional particulate superabsorbent polymers (SAPs) in cement paste by regulating the existence state of the polymer phase rather than modifying cement hydration chemistry. A basalt-polyacrylamide hydrogel composite (BCPA) was designed in which basalt particles functioned as physical crosslinking centers. Upon incorporation into cement paste, the composite did not significantly retard early hydration and exhibited a distinct microstructural response compared with chemically crosslinked polyacrylamide hydrogels. While typical SAP systems generate hydrogel-related macropores due to particle-scale swelling and subsequent volumetric collapse, the BCPA system showed a marked suppression of such macropores and a shift toward finer pore distributions. Correspondingly, the compressive strength loss was reduced from approximately 44% in conventional polyacrylamide-modified paste to about 20% with BCPA addition, while autogenous shrinkage at 7 days was reduced by roughly 75%, and cracking area was decreased by an order of magnitude. These results indicate that effective internal curing can be achieved with substantially reduced mechanical penalties compared with particulate hydrogel systems.

The combined interfacial, transport, and microstructural observations are consistent with an environmentally induced change in the polymer state within the cement matrix. Ionic shielding in the pore solution is inferred to weaken the original basalt-polymer association, which may lead to interfacial self-debonding and subsequent polymer redistribution. As a consequence, the polymer phase is considered to depart from discrete particle-scale domains, and contraction following water release is expected to occur over a reduced spatial scale. The resulting mitigation of hydrogel-related macropores allows internal curing functionality to be preserved while limiting microstructural deterioration. The present findings suggest that regulating polymer state and interfacial evolution offers a promising strategy for reconciling shrinkage mitigation with mechanical integrity in cement-based materials. It should be acknowledged that the proposed interfacial self-debonding and polymer redistribution mechanism is supported by converging indirect evidence, but has not been directly visualized in situ within the cement matrix. Accordingly, the proposed polymer state transition should be regarded as a mechanistic interpretation consistent with the combined experimental evidence rather than a directly proven process. Further work may proceed along several directions. Directly tracking the interfacial self-debonding and polymer redistribution through labeling-based or in situ visualization techniques, together with characterization of the local moisture gradient around the polymer phase, would help resolve the mechanism that the present study infers rather than directly observes. Extending the evaluation to long-term durability, to local mechanical characterization and dosage optimization, and to blended cementitious systems with different ionic environments and other hydrogel types including commercial acrylate-based products, would further clarify the robustness, design optimization, and applicability of this strategy. In addition, the present results are obtained on laboratory-prepared specimens, given that the raw materials are widely available and the processing route consists of simple and well-established operations, scaling up appears feasible, although practical factors related to large-scale production and compatibility with realistic concrete production will need to be further evaluated before engineering application.

CRediT authorship contribution statement

Yiqun Guo: Conceptualization, Funding acquisition, Methodology, Writing – original draft, Writing – review & editing. **Tongsheng Zhang:** Conceptualization, Writing – review & editing. **Yuwei Ma:** Funding acquisition, Writing – review & editing. **Tao Wang:** Methodology, Writing – review & editing. **Yunpeng Liu:** Investigation. **Mingxing Ni:** Investigation. **Guang Ye:** Writing – review & editing. **Jiangxiong Wei:** Writing – review & editing. **Jiyang Fu:** Funding acquisition, Writing – review & editing. **Qijun Yu:** Writing – review & editing.

Declaration of competing interest

The authors declare that they have no known competing financial interests or personal relationships that could have appeared to influence the work reported in this paper.

Acknowledgements

This work was funded by the National Natural Science Foundation of China (grant numbers 52572024, 52378227), Anhui Provincial Key Laboratory of Green and Low-Carbon Technology in Cement Manufacturing (grant number GLCT202404), State Key Laboratory of Silicate Materials for Architectures (Wuhan University of Technology) (grant number SYSJJ2024-05), Science and Technology of Guangdong Province (grant number 2025A0505020084), Science and Technology of Guangdong Province (No. 2023TQ07G174), and 111 Project (grant

number D21021). Their financial supports are gratefully acknowledged.

Data availability

Data will be made available on request.

References

[1] Tang S, Huang D, He Z. A review of autogenous shrinkage models of concrete. J Build Eng 2021;44:103412.
[2] Shen D, Shao H, Huang Y, et al. Influence of polyoxymethylene fibers on autogenous shrinkage, tensile creep, and cracking resistance of ultra-high performance concrete. Cement Concr Compos 2025;161:106090.
[3] Wang X, Yang Y, Zhong J. Novel strategy for autogenous shrinkage mitigation by combining internal curing and self-compensation: carbon nanotube sponge with carbamate solution absorbed. Cement Concr Compos 2025;157:105908.
[4] Liu J, Wang M, Liu N, et al. Development of ultra-fine SAP powder for lower-shrinkage and higher-strength cement pastes made with ultra-low water-to-binder ratio. Compos B Eng 2023;262:110810.
[5] Qin J, Dai F, Ma H, et al. Development and characterization of magnesium phosphate cement based ultra-high performance concrete. Compos B Eng 2022;234:109694.
[6] Zhao H, Ma Y, Zhang J, et al. Effect of clay content on shrinkage of cementitious materials. Constr Build Mater 2022;322:125959.
[7] Liu L, Fang Z, Huang Z, et al. Solving shrinkage problem of ultra-high-performance concrete by a combined use of expansive agent, super absorbent polymer, and shrinkage-reducing agent. Compos B Eng 2022;230:109503.
[8] Du J, Meng W, Khayat KH, et al. New development of ultra-high-performance concrete (UHPC). Compos B Eng 2021;224:109220.
[9] Li Y, Zhang C, Xiang Y, et al. Microstructure tailoring of internal curing agents: modified cement particles/superabsorbent polymers composites balancing strength and shrinkage mitigation. Cement Concr Res 2025;197:107950.
[10] Wyrzykowski M, Assmann A, Hesse C, et al. Microstructure development and autogenous shrinkage of mortars with C-S-H seeding and internal curing. Cement Concr Res 2020;129:105967.
[11] Zhang J, Bai S, Lyu J, et al. Synthesis of a spherical starch-based superabsorbent polymer and its influence on the microstructure of hardened cement paste. Compos B Eng 2025;297:112310.
[12] Jiang D, Li X, Li C, et al. Synergy between nano SiO_2-modified SAP and RHA in cement pastes: shrinkage, microstructure, and strength. Compos B Eng 2025;298:112368.
[13] Wu L, Farzadnia N, Shi C, et al. Autogenous shrinkage of high performance concrete: a review. Constr Build Mater 2017;149:62–75.
[14] Liu J, Farzadnia N, Khayat KH, et al. Effects of SAP characteristics on internal curing of UHPC matrix. Constr Build Mater 2021;280:122530.
[15] Kazemian M, Shafei B. Investigation of type, size, and dosage effects of superabsorbent polymers on the hydration development of high-performance cementitious materials. Constr Build Mater 2024;422:135801.
[16] Niu X, Zhang Y, Elakneswaran Y, et al. Effect of superabsorbent polymer (SAP) size on microstructure and compressive strength of concrete. Polymers 2024;16(2):197.
[17] Zhou B, Wang K, Taylor PC, et al. Superabsorbent polymers for internal curing concrete: an additional review on characteristics, effects, and applications. Materials 2024;17(22):5462.
[18] Vignesh J, Ramesh B, Xavier JR. Effects of nanomaterials on mechanical properties in cementitious construction materials for high-strength concrete applications: a review. J Adhes Sci Technol 2024;38(20):3737–68.
[19] Vignesh J, Ramesh B, Xavier JR. Recent advances in multifunctional nanocomposites for high-performance and durable concrete in harsh environments. Results Eng 2026;29:108840.
[20] Vignesh J, Ramesh B, Xavier JR. A comprehensive review of materials, processing, and performance of nano-doped engineered geopolymer composites for construction applications. Case Stud Constr Mater 2025;23:e05625.
[21] Vignesh J, Ramesh B, Xavier JR. Development of hybrid coating systems for concrete steel structures emphasizing fire protection and long-term durability. J Adhes Sci Technol 2026:1–67.
[22] Wang H, Lin J, Miao Y, et al. Hydrogel-guided dispersion strategy for enhancing the toughening efficiency of liquid polymers in cement paste. Cement Concr Res 2025;195:107926.
[23] Lin Q, Li H, Ji N, et al. Self-healing, stretchable, and freezing-resistant hydroxypropyl starch-based double-network hydrogels. Carbohydr Polym 2021;251:116982.
[24] Xu X, Jerca VV, Hoogenboom R. Bioinspired double network hydrogels: from covalent double network hydrogels via hybrid double network hydrogels to physical double network hydrogels. Mater Horiz 2021;8(4):1173–88.
[25] Hou D, Xu J, Zhang Y, et al. Insights into the molecular structure and reinforcement mechanism of the hydrogel-cement nanocomposite: an experimental and molecular dynamics study. Compos B Eng 2019;177:107421.
[26] Gao G, Du G, Sun Y, et al. Self-healable, tough, and ultrastretchable nanocomposite hydrogels based on reversible polyacrylamide/montmorillonite adsorption. ACS Appl Mater Interfaces 2015;7(8):5029–37.
[27] Krafcik MJ, Bose B, Erk KA. Synthesis and characterization of polymer-silica composite hydrogel particles and influence of hydrogel composition on cement paste microstructure. Adva Civil Eng Mater 2018;7(4):590–613.
[28] Jiang D, Li X, Zhao P, et al. Internal curing with superabsorbent polymer modified by nano SiO_2: shrinkage mitigation and microstructure refinement. Cement Concr Res 2024;175:107353.
[29] Bose B, Davis CR, Erk KA. Microstructural refinement of cement paste internally cured by polyacrylamide composite hydrogel particles containing silica fume and nanosilica. Cement Concr Res 2021;143:106400.
[30] Yang J, Meng S, Xu L, et al. Water adsorption on hydroxylated silica surfaces studied using the density functional theory. Phys Rev B 2005;71(3):035413.
[31] Dannert C, Stokke BT, Dias RS. Nanoparticle-hydrogel composites: from molecular interactions to macroscopic behavior. Polymers 2019;11(2):275.
[32] Zareie C, Bahramian AR, Sefti MV, et al. Network-gel strength relationship and performance improvement of polyacrylamide hydrogel using nano-silica; with regards to application in oil wells conditions. J Mol Liq 2019;278:512–20.
[33] Salleh KM, Zakaria S, Sajab MS, et al. Chemically crosslinked hydrogel and its driving force towards superabsorbent behaviour. Int J Biol Macromol 2018;118:1422–30.
[34] Zhao L, Huang J, Zhang Y, et al. Programmable and bidirectional bending of soft actuators based on janus structure with sticky tough PAA-Clay hydrogel. ACS Appl Mater Interfaces 2017;9(13):11866–73.
[35] Schröfl C, Mechtcherine V, Gorges M. Relation between the molecular structure and the efficiency of superabsorbent polymers (SAP) as concrete admixture to mitigate autogenous shrinkage. Cement Concr Res 2012;42(6):865–73.
[36] Schroefl C, Mechtcherine V, Vontobel P, et al. Sorption kinetics of superabsorbent polymers (SAPs) in fresh Portland cement-based pastes visualized and quantified by neutron radiography and correlated to the progress of cement hydration. Cement Concr Res 2015;75:1–13.
[37] Tenório Filho JR, de Araújo MAPG, Mannekens E, et al. Alginate- and sulfonate-based superabsorbent polymers for application in cementitious materials: effects of kinetics on internal curing and other properties. Cement Concr Res 2022;159:106889.
[38] Zhong P, Hu Z, Griffa M, et al. Mechanisms of internal curing water release from retentive and non-retentive superabsorbent polymers in cement paste. Cement Concr Res 2021;147:106494.
[39] Albert C, Isgor OB, Angst U. Exploring machine learning to predict the pore solution composition of hardened cementitious systems. Cement Concr Res 2022;162:107001.
[40] Lv B, Wang L, Zeng Q, et al. Autogenous shrinkage mitigation effect of superabsorbent polymers on alkali-activated GGBFS-FA binary binder without additional water: performance, microstructure and mechanism. Cement Concr Res 2026;199:108058.
[41] Li J, Che D, Liu Z, et al. Effect of basalt powder on hydration, rheology, and strength development of cement paste. Materials 2022;15(23):8632.
[42] Mechtcherine V, Snoeck D, Schröfl C, et al. Testing superabsorbent polymer (SAP) sorption properties prior to implementation in concrete: results of a RILEM round-robin test. Mater Struct 2018;51(1):28.
[43] Guo Y, Zhang T, Du J, et al. The chloride binding capacity and stability of gap-graded blended cement with calcined hydrotalcite and metakaolin. J Build Eng 2022;49:104093.
[44] Mao Y, Drissi S, He P, et al. Quantifying the effects of wet carbonated recycled cement paste powder on the properties of cement paste. Cement Concr Res 2024;175:107381.
[45] Guo Y, Zhang T, Du J, et al. Evaluating the chloride diffusion coefficient of cement mortars based on the tortuosity of pore structurally-designed cement pastes. Microporous Mesoporous Mater 2021;317:111018.
[46] Gao P, Zhang T, Luo R, et al. Improvement of autogenous shrinkage measurement for cement paste at very early age: corrugated tube method using non-contact sensors. Constr Build Mater 2014;55:57–62.
[47] Ma Y, Yang X, Hu J, et al. Accurate determination of the “time-zero” of autogenous shrinkage in alkali-activated fly ash/slag system. Compos B Eng 2019;177:107367.
[48] Landrou G, Brumaud C, Plötze ML, et al. A fresh look at dense clay paste: deflocculation and thixotropy mechanisms. Colloids Surf A Physicochem Eng Asp 2018;539:252–60.
[49] Fu X, Yang Q, Zhang Y. Thermal decomposition behavior and mechanism study of cationic polyacrylamide. J Therm Anal Calorim 2021;146(3):1371–81.
[50] Gutch PK, Jitendra S, Alankar S, et al. Thermal analysis of interaction between 2-PAM chloride and various excipients in some binary mixtures by TGA and DSC. J Therm Anal Calorim 2013;111(3):1953–8.
[51] Mohammadi M, Khorrami MK, Ghasemzadeh H. ATR-FTIR spectroscopy and chemometric techniques for determination of polymer solution viscosity in the presence of SiO_2 nanoparticle and salinity. Spectrochim Acta Mol Biomol Spectrosc 2019;220:117049.
[52] Mao Q, Li Y, Liu K, et al. Mechanism, characterization and factors of reaction between basalt and alkali: exploratory investigation for potential application in geopolymer concrete. Cement Concr Compos 2022;130:104526.
[53] Shettigar RR, Misra NM, Patel K. CTAB grafted PAM gel and its application in drilling fluid. J Petrol Sci Eng 2018;160:129–35.
[54] Shi Z, Ma Q, Liu X, et al. Design and manufacture of structure-function integrated carbon fiber reinforced plastics for composite construction. Compos B Eng 2025;291:112030.
[55] Du J, Zhang T, Chen P, et al. Phase separation of recycled concrete powder during grinding and consequent influences on its hydration behaviors in cement paste. Cement Concr Compos 2023;142:105203.
[56] Yuan Q, Xie Z, Yao H, et al. Hydration, mechanical properties, and microstructural characteristics of cement pastes with different ionic polyacrylamides: a comparative study. J Build Eng 2022;56:104763.

[57] Li X, Yan J, Ma W, et al. Comparative study on the properties of cement grout modified with PAM and PANA at elevated temperatures. Powder Technol 2024; 433:119256.
[58] Holt E. Contribution of mixture design to chemical and autogenous shrinkage of concrete at early ages. Cement Concr Res 2005;35(3):464–72.
[59] Guan X, Zhang J, Zhao S. Design, synthesis and characterization of a starch-based superabsorbent polymer and its impact on autogenous shrinkage of cement paste. Constr Build Mater 2024;415:134986.
[60] Hiller DS, Seshadri AN, Schröfl C, et al. Shrinkage mitigation and mechanical properties of cement-based mortar with silane-functionalized hydrogels. J Appl Polym Sci 2026;143(14):e70420.
[61] Chai H, Zhang H, Hou C, et al. Experimental study on chloride corrosion resistance of sulphoaluminate cement modified by acrylamide in situ polymerization. J Build Eng 2023;73:106730.
[62] Qi W, Zhang S, Fang Z, et al. Effect of maintenance environment on the mechanical property and pore structure of cement paste mixed by seawater. Constr Build Mater 2024;418:135280.
[63] Long S, Chen F, Ren H, et al. Ion-cross-linked hybrid photochromic hydrogels with enhanced mechanical properties and shape memory behaviour. Polymers 2024;16 (8):1031.
[64] Yan S, Shao L, Shu L, et al. Performance and mechanism of dual-network cementitious material formed by acrylamide monomer in-situ polymerization and ultra-fine portland cement. J Mater Sci 2024;59(29):13709–23.